Polito *et al. Biology Direct* (2024) 19:91
https://doi.org/10.1186/s13062-024-00540-8

Biology Direct

RESEARCH Open Access

Biochemical characterization of the feedforward loop between CDK1 and FOXM1 in epidermal stem cells

Maria Pia Polito[1†], Alessio Romaldini[1†], Lorenzo Tagliazucchi[2], Grazia Marini[1], Federica Radice[1], Gaia Andrea Gozza[1], Giulia Bergamini[1], Maria Paola Costi[2] and Elena Enzo[1*]

Abstract

The complex network governing self-renewal in epidermal stem cells (EPSCs) is only partially defined. FOXM1 is one of the main players in this network, but the upstream signals regulating its activity remain to be elucidated. In this study, we identify cyclin-dependent kinase 1 (CDK1) as the principal kinase controlling FOXM1 activity in human primary keratinocytes. Mass spectrometry identified CDK1 as a key hub in a stem cell-associated protein network, showing its upregulation and interaction with essential self renewal-related markers. CDK1 phosphorylates FOXM1 at specific residues, stabilizing the protein and enhancing its nuclear localization and transcriptional activity, promoting self-renewal. Additionally, FOXM1 binds to the CDK1 promoter, inducing its expression.

We identify the CDK1-FOXM1 feedforward loop as a critical axis sustaining EPSCs during in vitro cultivation. Understanding the upstream regulators of FOXM1 activity offers new insights into the biochemical mechanisms underlying self-renewal and differentiation in human primary keratinocytes.

Keywords Phosphorylation, FOXM1, CDK1, Epidermal stem cell

Introduction

The epidermis is the outermost layer of the skin, consisting of a stratified epithelial structure that shields the human body from external factors and prevents water loss. The basal layer of the epidermis is tightly connected to the underlying dermis, and it is composed by both epidermal stem cells (EPSCs) and transient amplifying progenitors (TACs) [1, 2]. EPSCs are long-lived, stem cells that sustain timely repair and long-term regeneration of the tissue [3–5]. They give rise to TACs, which undergo a process of terminal differentiation to spinous, granular, and cornified layers [6]. The careful regulation of keratinocyte proliferation and differentiation is crucial for preserving epidermal balance. When the skin is injured, this balance is disrupted, and keratinocytes at the wound edge rapidly alter their function to participate in tissue repair [7].

EPSCs can be in vitro expanded to generate a functional epithelial graft and an adequate number of these cells guarantees long-term epithelial regeneration in the patient [3, 8–11]. It has already been proven that EPSCs can be genetically corrected to treat genetic skin disease such as different types of epidermolysis bullosa (EB) and lamellar ichthyosis (LI) [3, 11–14]. Thus, a thorough

[†]Maria Pia Polito and Alessio Romaldini contributed equally to this work.

*Correspondence:
Elena Enzo
elena.enzo@unimore.it
[1]Centre for Regenerative Medicine "Stefano Ferrari", Department of Life Science, University of Modena and Reggio Emilia, Via Glauco Gottardi 100, Modena, Italy
[2]Department of Life Sciences, University of Modena and Reggio Emilia, Via Campi 103, Modena 41125, Italy

understanding of the biochemical mechanisms governing self-renewal during in vitro cultivation could help to unveil potential molecular targets for treating skin disorders due to aberrant keratinocyte proliferation and differentiation programs, such as psoriasis and skin cancer [15–19].

During in vitro cultivation, EPSCs give rise to clones identified as holoclones [3], while TACs are identified as meroclone- and paraclone-forming cells [20]. The first important step in the identification of the biochemical differences among the three types of clones derives from the discovery of TP63, which is required for squamous epithelia development [21, 22]. TP63 is highly expressed in holoclones, where it sustains the proliferative potential, driving the expression of epithelial-specific markers, metabolic genes and long noncoding RNA [23–27]. Further insight into the network controlling EPSCs, TACs, and differentiated cells derives from a combination of microarray analysis and single-cell sequencing data [28, 29]. It has been demonstrated that YAP signaling is required for self-renewal in EPSCs, and it promotes the expression of the transcription factor FOXM1 [28, 30]. FOXM1 induces the expression of Histone linker H1 isoform B (namely H1B), a protein that plays a pivotal role in DNA packaging and gene expression regulation. In EPSCs, H1B is associated with promoters of differentiation-related genes, maintaining their silencing and thereby preserving the undifferentiated state [31]. FOXM1 activity is intricately controlled by phosphorylation, but the kinases responsible for such regulation in EPSCs have not been identified yet [32–34]. Uncovering the biochemical pathways upstream of FOXM1 could be crucial for effectively modulating its function.

Cyclin-dependent kinases (CDKs) are serine/threonine kinases whose activity is regulated by their association with cyclins and inhibited by CDK inhibitors (CKIs). In their monomeric, inactive form, CDKs have a two-lobed structure: a conserved catalytic core with an ATP-binding pocket flanked by a PSTAIRE-like cyclin-binding domain and an activating T-loop motif [35, 36]. In mammals, CDKs are categorized into cell-cycle-related (CDK1, CDK2, CDK4, CDK6) and transcription-related (CDK7, CDK8, CDK9, CDK11, CDK20) groups [36, 37].

CDK1, while primarily known for its role in cell cycle progression, is involved in many other processes, such as signal expression regulation, apoptosis, mitochondrial function, Golgi remodeling, and intermediate filaments organization, as reviewed in Massacci et al. [38]. Many of these functions are closely linked to stem cell self-renewal. For instance, during the development of embryonic stem cells (ESCs), CDK1 interacts with Oct4 to prevent differentiation into the trophectoderm lineage [35, 39]. During neurogenesis, CDK kinases are crucial for the multi-site phosphorylation of the Neurogenin 2 transcription factor, thereby inhibiting neurogenic gene expression [40]. In myoblasts, CDK1 and CDK2 phosphorylate MyoD, enhancing its turnover and promoting the maintenance of a proliferative state [41]. Additionally, CDK1 downregulation leads to premature differentiation and accumulation of chromosomal alteration [42].

Human primary epidermal cultures can provide an ideal model for studying CDK1 role in self-renewal and differentiation. Previous studies reported that FOXM1 activity is regulated by CDK1 in cancer cell lines [43, 44]; however, CDK1's role in the epithelial stem cell biology remains largely unexplored.

In this work, we took advantage of a label free bottom-up mass spectrometry (MS) proteomic to study the proteomic profile of stem-cell enriched versus stem-cell depleted keratinocyte cultures. CDK1 emerged as a central player that could positively regulate FOXM1 activity in EPSCs. Hampering CDK1 and FOXM1 activity by means of specific inhibitors and CRISPR-Cas9 technology, we pointed out CDK1 as one of the major kinases responsible for FOXM1 phosphorylation and stabilization. In addition, we found that FOXM1 binds to the CDK1 promoter, probably inducing its expression and engaging in a positive loop that could sustain self-renewal in EPSCs.

Methods

Human tissues

All human tissues were collected after informed consent for use of tissues in research and in compliance with Italian regulations (Comitato Etico dell'Area Vasta Emilia Nord, number 178/09 for healthy donor skin samples and number 124/2016 skin biopsies obtained from patients affected by JEB).

Primary human cell cultures from healthy donors and JEB patient

Human skin samples from surgical waste (abdominoplasty or mammoplasty) were collected and anonymized. Briefly, skin biopsies were minced and treated with 0.05% trypsin/0.01% EDTA for 4 h at 37 °C. Every 30 min keratinocytes were collected, plated ($2.5–3\times10^4$/cm^2) on lethally irradiated 3T3-J2 cells (2.4×10^4/cm^2), and grown at 37 °C, 5% CO_2 in humidified atmosphere in keratinocyte growth medium (KGM), comprising Dulbecco's modified Eagle's (DMEM) and Ham's F12 media (2:1 mixture) containing fetal bovine serum (FBS, 10%), penicillin–streptomycin (50 IU/ml), glutamine (4 mM), adenine (0.18 mM), insulin (5 mg/ml), cholera toxin (0.1 nM), hydrocortisone (0.4 mg/ml), triiodothyronine (Liothyronine Sodium, 2 nM), epidermal growth factor (EGF, 10 ng/ml). When subconfluent, cell cultures were serially propagated until senescence. A skin biopsy (1 cm^2)

has been collected from a LAMB3-dependent JEB patient (1-month-old) and cultivated as described above.

3T3-J2 cell line

Mouse 3T3-J2 cells were a gift from Prof. Howard Green, Harvard Medical School (Boston, MA, USA). Fibroblasts were cultivated in DMEM supplemented with 10% gamma-irradiated donor adult bovine serum, penicillin–streptomycin (50 IU/ml) and glutamine (4 mM) [45].

Sample processing for MS proteomics analysis

Samples were treated as described in d'Arca et al. [46], with slight modifications. After feeder layer removal, scraped cells were resuspended in 0.6 mL of 1X RIPA buffer (Sigma Aldrich) supplemented with Protease Inhibitor (Thermo Fisher) and Phosphatase Inhibitor (Thermo Fisher) cocktails, vortexed, incubated overnight at -80 °C, and centrifuged at 14,000 g for 10 min at +4 °C. Supernatants were collected and their protein content was quantified using the BCA assay (Thermo Fisher). A volume equivalent to 35 µg of protein lysate per sample was loaded into Millipore 30 kDa MWCO centrifugal filters (Merck). It was heat-denatured with a Thermomixer (Eppendorf), reduced with excess dithiothreitol, and cys-alkylated with iodoacetamide. Then 1 µg MS grade trypsin (Roche, Basel, Switzerland) was added for protein digestion. The obtained samples were recovered from the filters with 50 µL of 0.5 M NaCl, buffered with TFA and desalted throught C18 SPE columns (Empore 3 M – CDS Analytical, PA, U.S.). The eluted peptides were lyophilized in a SpeedVac (Eppendorf). Samples were stored at -80 °C until MS analysis. Three independent NHK primary cultures were processed as described above (biological replicates). Each sample was digested and divided in two technical replicates.

MS proteomics analysis

1µg of peptide per sample was injected on a UltiMate 3000 RSLCnano UHPLC coupled to an Orbitrap Exploris 480 Mass Spectrometer (Thermo Fisher Scientific), equipped with a nano-ESI source. An EASY-Spray 500 mm x 75 µm, ID 2 µm, column was employed for sample separation at 20 µL/min in a 160 min gradient (2 to 30% ACN in 0.1% formic acid), with a FullMS-ddMS^2 method, (top20), in positive ionization mode. This allowed for the fragmentation of the most intense 20 ions per MS^1 scan. Analysis parameters were set as follows: MS^1 resolution 120,000, Scan range 375–3000, RF lens 50%, normalized ACG target 300%, MaxIT 120ns, 2–5 charge state. MS/MS parameters were set as follows: NCE 30%, isolation window 1.5 m/z, isolation offset 0.4 m/z, normalized ACG target 200% (120ns MaxIT). Dynamic exclusion option was used throughout all the experiment with a 55s window to maximize peptide identification. The reliability of chromatograms in terms of intensity (Total ion current) and peptide separation (resolution) was manually annotated with FreeStyle tool (Thermo Fisher Scientific).

MS data analysis

The raw data files were analyzed with Proteome Discoverer v3.1 (Thermo Fisher Scientific) [47]. Excel file reporting the raw data (normalized protein intensity values) of the Label Free MS Proteomics experiment and the differentially expressed proteins (DEPs) is available in Open Access on the FairDom repository at https://fairdomhub.org/data_files/7500 upon request to the authors. Peptides from each sample were searched against a FASTA database built with UniProt [48] 20,431 annotations from *H. sapiens* and 115 from the Common Repository of Adventitious Proteins database (cRAP) for contaminants identification [49]. *q*-value (*p*-value adj. to FDR < 1% acc. to Benjamini correction) was used for peptide matching. Threshold parameters employed for protein identification were set as follows: 10ppm for precursor ion, 0.02Da for fragment ions, max 1 missed cleavage, $1\times^{13}C$ isotope, Cys- carbamidomethylation as fixed modification, and M-oxidation as variable modification. The pipeline of protein identification includes peptide matching with SEQUEST algorithm, and rescoring with Chimerys v4.0, per each sample independently [50]. Proteins matched with a coverage ≥ 5%, and proteins identified with ≥ 2 peptides (> 1 unique) were included in protein identification as reliable hits. Peptide quantitation was performed after sample normalization with an interval of confidence 95% around the average total ion current, by encompassing precursor ion intensities. A *t*-test was applied between the enriched sample group and the depleted sample group to score the ratios of protein expression (*q*-values). Contaminants from the cRAP database and murine fibroblast from the cell matrix were excluded from the quantitation. A preliminary analysis between all the murine fibroblast and the human keratinocyte proteome was performed to assess that no mismatch in peptide identification interspecies was occurring.

Bioinformatic analysis of MS data

Protein localization distribution (Gene Ontology- Cellular Component) was obtained with the GO extension on Proteome Discoverer, according to their percentage of representation (cumulative). A g: Profiler functional profiler analysis (g: GOSt) was run on the genes corresponding to the DEPs (Ensembl Gene ID extension was used for conversion, Provided by Proteome Discoverer and available on Suppl. Table 1) to characterize the main GOs and biological processes involved in cell metabolism. STRING network enrichment web tool was used to evaluate the biochemical crosstalk of the DEPs

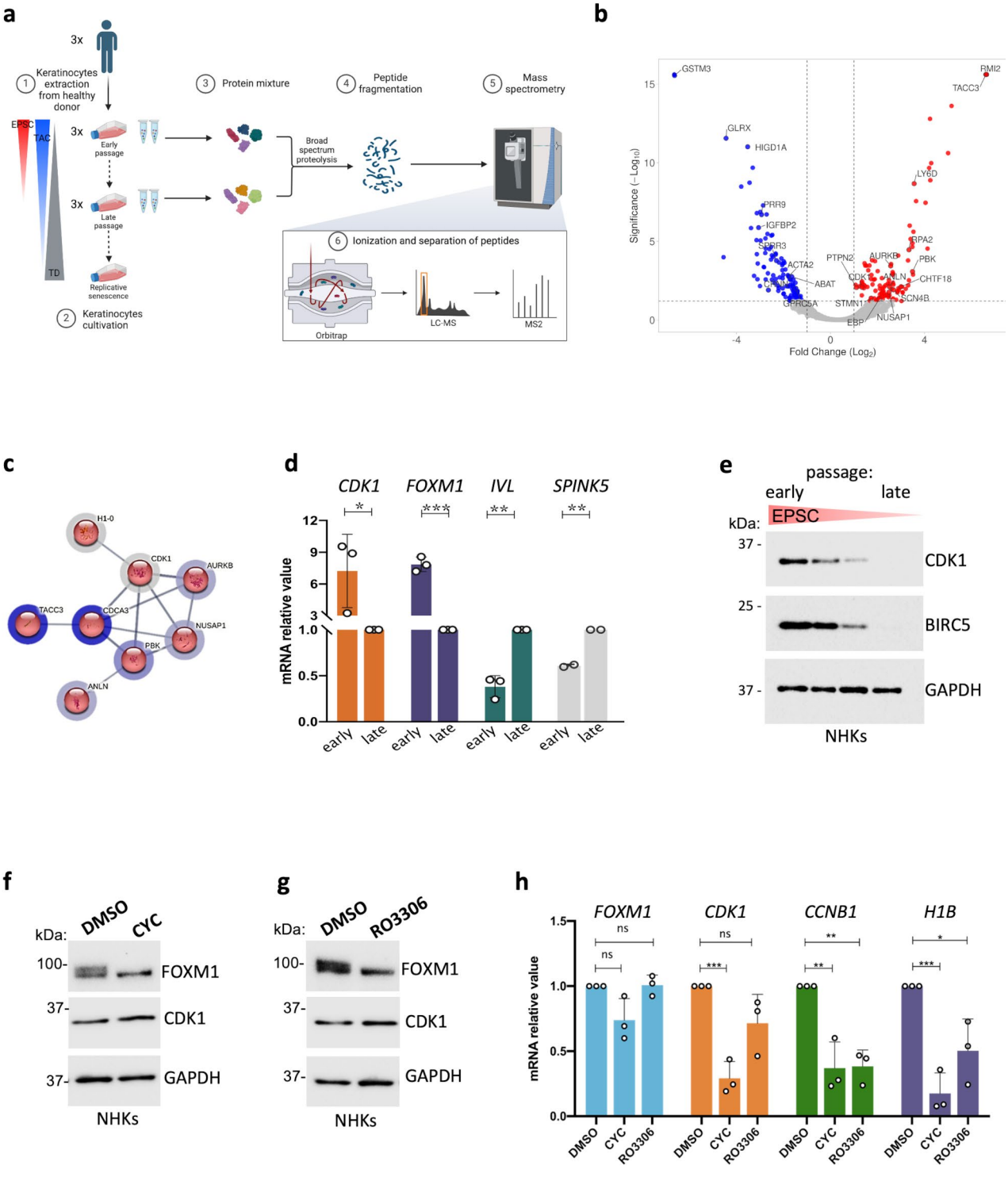

Fig. 1 (See legend on next page.)

and the sub-networks through the MCL local network analysis. Briefly, all the DEPs for the MS analysis were uploaded on STRING with their corresponding fold change values and analyzed with a medium confidence level (0.400) in a global network analysis. The MCL algorithm was used to generate local networks according to their inflation parameters, and the cluster surrounding

(See figure on previous page.)

Fig. 1 CDK1 is upregulated in stem-cell enriched epidermal cultures. (**a**) Scheme describing the experimental pipeline for mass spectrometry analysis; abbreviations: EPSC = Epidermal Stem Cell, TAC = Transient Amplifying Cell, TD = Terminally Differentiated cell, LC-MS = Liquid Chromatography Mass Spectrometry; MS = Mass Spectrometry; (**b**) Volcano plot representation of the proteins identified by the MS proteomics analysis of enriched vs. depleted samples. Significantly downregulated proteins are represented in blue, significantly upregulated proteins are represented in red. On X-axis, Fold-change is reported (log_2(ratio)), while on Y-axis proteins' significance is depicted (as -Log_{10} of the corresponding *q*-value). (**c**) STRING local Network analysis (LNA) obtained from the MCL cluster. Number of nodes: 8, number of edges: 12, average node degree: 3, avg. local clustering coefficient: 0.792, expected number of edges: 0, PPI enrichment *p*-value: 2.11×10^{-15}. (**d**) qRT-PCR quantification of the mRNA levels of *CDK1*, *H1B*, *IVL*, and *SPINK5* on three different NHK primary cultures. Expression levels were normalized per *GAPDH*. Data are presented as mean +/− SD of $N = 3$ different independent biological replicates, $^{*}P < 0.05$ (Student *t*-test). (**e**) Western analysis of total cell extracts from cultures generated by sub-confluent NHKs during serial cultivation. Molecular weight indicators are shown. (**f**) Western analysis of total cell extracts derived from NHK cultures treated with 30 µM CYC (see Methods) or DMSO as control. Molecular weight indicators are shown. (**g**) Western analysis of total cell extracts derived from NHK cultures treated with 30 µM RO3306 (see Methods) or DMSO as control. Molecular weight indicators are shown. (**h**) qRT-PCR quantification of the mRNA levels of *FOXM1*, *CDK1*, *CCNB1*, and *H1B* on cells derived from DMSO-, CYC- or RO3306-treated NHK cultures. Expression levels were normalized per *GAPDH* and given relative to the control (DMSO) arbitrarily set to 1. Data are presented as mean +/− SD of $N = 3$ different independent biological replicates, $^{*}P < 0.05$, $^{**}P < 0.01$, $^{***}P < 0.001$, *ns* = not significant (Student *t*-test)

CDK1 is reported in Fig. 1c with the corresponding GOs descriptors.

Clonal analysis

Sub-confluent keratinocyte mass cultures were trypsinized and 0.5–1 cell was plated into each well of a 96-well plate after serial dilution. Single clones were cultivated for 7 days and treated with 0.05% trypsin and 0.01% EDTA at 37 °C for 15–20 min. One-quarter of the clone was plated into an indicator dish, cultivated for 12 days, and stained with rhodamine B to classify the clonal type. The remaining three-quarters were sub-cultivated into an adequate plastic support and used for further analyses [51].

Western blotting

Feeder layer was mechanically removed by sprinkling on top 20 mM cold PBS/EDTA. Keratinocytes were collected by scraping in 1× RIPA buffer (Sigma Aldrich) supplemented with Phosphatase and Protease Inhibitor Cocktails (Thermo Fisher). Pierce BCA Protein Assay kits (Thermo Scientific) were used to quantify the total protein amount. The same amount of proteins was loaded in 4–12% NuPAGE Bis-Tris Gels and transferred using 100 V at 4 °C for 2 h onto the nitrocellulose membrane (Millipore). Membranes were treated with Everyblot blocking solution (Bio-Rad). Primary antibodies were diluted in Everyblot blocking solution (Bio-Rad) as indicated in Suppl. Tables 4 and added overnight at 4 °C to the membranes. Secondary antibodies were diluted in Everyblot blocking solution (Bio-Rad) as indicated in Suppl. Tables 4 and added to the corresponding membranes for 1 h at room temperature. Signal was visualized with Clarity Western ECL substrate (Bio-Rad) using ChemiDoc (Bio-Rad) and ImageLabs software. Gray background on the images was homogeneously added for graphical purposes.

RNP complex formation and nucleofection

The synthetic guide was designed on the exon 2 of FOXM1 genomic sequence (5′-CATGCCCAACACG CAAGTAG −3′) and directly flanking a TGG PAM. It was purchased by Thermo Fisher Scientific (Assay ID CRISPR739962_SGM, Cat. #A35533). A non-targeting guideRNA was used as in [13]. SgRNA was mixed with SpCas9 (Alt-R S.p. Cas9 Nuclease V3, IDT, #1081058) and P3 Primary Cell Nucleofector® Solution to attain a molar ratio 1,15:1 of sgRNA to SpCas9. Then 1×10^5 keratinocytes were resuspended in 20 µL of supplemented NucleofectorTM Solution at RT, 5 µL of the RNP and 1 µL of 100 µM Alt-R Cas9 Electroporation Enhancer (Alt-R Cas9 Electroporation Enhancer, IDT, #1075915). Cells were transferred to 16-well Nucleocuvette® Strips and electroporated using a 4D-Nucleofector (4D-Nucleofector Core Unit, Lonza, #AAF-1001B; 4D-Nucleofector X Unit, Lonza, #AAF-1001X) using the program DS-138.

TIDE (Tracking of indels by decomposition) analysis

Genomic DNA was extracted from sub-confluent normal human primary keratinocyte (NHK) cultures and the locus around the deletion was amplified by PCR (see Suppl. Table 5 for primers sequences) and used to perform Sanger sequencing. The resulting sequence trace files were uploaded on the TIDE web tool with the guide RNA sequence as input (sensitivity > 1–5%).

Binding sites analysis

To predict potential binding sites for the transcription factor FOXM1 in the promoter region of the *CDK1* gene, the Biostrings package on R was used. The FOXM1 binding motif was retrieved from Jaspar website (https://jaspar.uio.no/) (ID: UN0802.1). Promoter sequence of the *CDK1* gene was obtained from UCSC Genome Browser (1 kb upstream TSS). *MatchPattern* function was used to scan for FOXM1 motif occurrences in the promoter sequence, allowing a maximum mismatch = 1.

Chromatin immunoprecipitation

For chromatin immunoprecipitation, iDeal ChIP-seq kit for Transcription Factors from Diagenode (Cat. No.: C01010055) was used following the manufacturer's instruction. Briefly, cells were crosslinked with 1% formaldehyde (Sigma) in culture medium for 10 min at room temperature, and chromatin from lysed nuclei was sheared to 200–600 bp fragments using a Branson Sonifier. Chromatin derived from 4×10^6 cells was incubated with indicated antibodies (Suppl. Table 4) overnight at 4 °C. Antibody/antigen complexes were recovered with ProteinA/G beads for 2 h at 4 °C. Quantitative real-time PCR was carried out on a QuantStudio 12k Flex Real-Time PCR System (Thermo Fisher) with custom-made oligonucleotides and PowerUP SYBR green master mix (Thermo Fisher); each sample was analyzed in triplicate. The amount of immunoprecipitated DNA in each sample was determined as the fraction of the input (amplification efficiency (Ct INPUT_Ct ChIP)). Primers are listed in Suppl. Table 5.

RNA extraction and droplet digital PCR (ddPCR)

For real-time qPCR, total RNA was isolated from cultured cells using the PureLink RNA Mini Kit (Thermo Fisher). Complementary DNA (cDNA) was generated using the SuperScript VILO cDNA Synthesis Kit (Thermo Fisher). ddPCR was carried out on the reverse transcribed cDNA using QX200™ ddPCR™ EvaGreen Supermix (BioRad) or ddPCR™ Supermix for Probes (BioRad). To generate individual reaction droplets, QX200™ Droplet Generator was used. The droplets were then transferred to a sealed polymerase chain reaction (PCR) plate to conduct thermal cycling according to the assay requirements. Finally, the QX200™ Droplet Reader was used to measure the fluorescence in each droplet. Data were analyzed using QuantaSoft™ Analysis Pro software and visualized with Prism 8. List of Taqman Probes (Thermo Fisher) used is provided in Suppl. Table 6.

Drug treatments

R-Roscovitine or CYC202 (HY-30237), RO3306 (HY-12529), and FDI-6 (HY-112721) were added to NHKs after three days of culture. The three drugs were firstly resuspended in DMSO and then diluted in culture medium to a final concentration of 30 µM. NHKs treated with RO3306 were harvested after 6 h, and NHKs treated with CYC202, and FDI-6 were harvested after 24 h. All three drugs were purchased from MedChem.

Flow cytometry biparametric staining for cell-cycle analysis

Cell-cycle analysis was performed using Click-iTTM EdU Flow Cytometry Assay Kit by Invitrogen according to the manufacturer's protocol. In brief, cells were incubated with EdU diluted 1:1000 for 2 h, harvested, and stained for 3t3-feeder cells. They were then fixed, permeabilized, incubated with Click-iT reaction cocktail and eventually stained with FxCycleTMViolet. Stained cells were analyzed with BD FACSCanto II, BD FACSDiva Software v6.1.3, and FlowJo v10.

Single cell transcriptomic profile and bioinformatic analysis

For details on single-cell RNA sequencing experiments refer to Enzo et al., 2021 [28]. Briefly, two keratinocyte cultures were detached with trypsin for 15–20 min to obtain a single cell suspension, pelleted, and resuspended in culture medium and in 0.04% BSA in 1X PBS. For each sample, 1.0×10^4 cells were loaded into one channel of the Chromium Chip B using the Single Cell reagent kit v3 (10X Genomic). cDNA was synthesized and amplified for 14 cycles following the manufacturer's protocol. Sequencing was performed on the NextSeq550 Illumina sequencing platform, reaching at least 50,000 reads as mean reads per cell. The Cell Ranger Count pipeline (version 3.1.0) was used to align reads of the dataset to the reference transcriptome (GRCh38) and to calculate UMI counts from the mapped reads. Expression data were imported in R and analyzed using Seurat (version 4.3.0) R package. 3,367 and 3,978 cells were obtained from two independent sub-confluent primary epidermal cultures. Single-cell transcriptomic data of healthy-donor-derived skin biopsy were processed using the same procedure described above, retrieving 8,570 cells, as described in [31]. Cells were classified using the annotated dataset as reference and the *FindTransferAnchors* and *TransferData* functions in Seurat with default parameters. Seurat *MapQuery* function was used to project the healthy-donor-derived skin biopsy dataset onto the reference UMAP structure.

For the co-expression analysis, data were normalized using the *NormalizeData* function in Seurat. Expression levels for *FOXM1* and *CDK1* were extracted, with an expression threshold set at >0. Colocalization was identified when the expression levels of both genes exceeded this threshold. Starting from the normalized data, the average expression for each cluster was calculated using the *AverageExpression* function in Seurat.

Results

Mass spectrometry analysis of stem cell-enriched versus stem cell-depleted epithelial cultures

Normal human primary keratinocyte (NHK) cultures were established from biopsies obtained from three skin biopsies derived from healthy donors and serially cultivated to explore changes in protein expression during clonal conversion. Early-passage cultures contain the highest proportion of stem cells with minimal differentiation. As passages progress, stem cells are progressively

depleted and replaced by TACs and differentiated cells as a result of clonal conversion (Fig. 1a).

To identify proteins that are differentially expressed during clonal conversion, we performed liquid chromatography-tandem mass spectrometry (LC-MS/MS) proteomic analysis on early- and late-passage NHK cultures (Fig. 1a). A total of 5,437 proteins were identified (Suppl. Figure 1a, b, c). Most of these proteins were localized in the nucleus (65% of total), followed by membrane (48%), and cytoskeletal components (47%) (cumulative percentages; Suppl. Figure 1d).

Among the identified proteins, 289 were significantly differentially expressed ($q<0.05$, Abundance Ratio > 2), with 142 proteins upregulated and 147 proteins downregulated in early-passage cultures as compared to late-passage ones (Fig. 1b, Suppl. Table 1). The functional enrichment analysis using g: Profiler revealed that the upregulated proteins were associated with cellular components such as the endoplasmic reticulum (GO:0005789) and chromosome organization (GO:0051276), as well as biological processes like DNA replication and base excision repair (REAC: R-HSA-73884) (Suppl. Table 2). Conversely, proteins upregulated in later passages were primarily linked to the cytoplasmic component (GO:0005737) and ATP metabolic processes (GO:0046034) (Suppl. Table 3).

STRING analysis with Local Network Analysis (LnA) of the primary cluster identified by the Markov Cluster Algorithm (MCL) revealed a key protein interaction network ($p=4.37\times10^{-6}$) consisting of eight proteins (Fig. 1c). Seven of these proteins (ANLN, AURKB, NUSAP1, TACC3, PBK, CDCA3, and CDK1) have been previously associated with the "holoclone signature" as potential markers of holoclone-forming stem cells [28]. The eighth protein, H1-0, belongs to the histone H1 linker family. Although the role of H1B in epidermal stem cell biology has been explored [31], the function of the H1-0 isoform remains to be further investigated.

Notably, CDK1 emerged as a central hub in this network, showing overexpression (fold change 1.34, ratio 2.54; Fig. 1b) and medium-strength interactions (significance = 0.400) with other stem cell-associated proteins in early-passage samples compared to late-passage samples ($q=9.27\times10^{-3}$, Fig. 1c, Suppl. Figure 1e). This data suggests that CDK1 may play a role in sustaining stem cell properties during early stages of cultivation. Consequently, we focused on further investigating CDK1 function, particularly as a potential upstream regulator of FOXM1, a key transcription factor involved in stem cell maintenance [28].

CDK1 phosphorylates FOXM1 in human primary keratinocytes

Building on these insights, we sought to further elucidate the role of CDK1 in early-passage cultures, hypothesizing that CDK1 may act as a key kinase for FOXM1. To validate the MS findings, we assessed CDK1 expression at both RNA and protein levels in early- and late-passaged NHKs. As expected, early passages exhibited increased *FOXM1* mRNA expression along with decreased expression of differentiation markers, such as *SPINK5* and *IVL*, compared to late passages (Fig. 1d). Correspondingly, *CDK1* mRNA levels were higher in early passages and significantly reduced in late passages. This trend was also evident at the protein level, where CDK1 expression decreased progressively with serial cultivation, mirroring the decline of the stem-cell marker BIRC5 (Fig. 1e).

FOXM1 has been shown to play a critical role in maintaining epidermal stem cells and is essential for holoclone-forming cell maintenance during in vitro cultivation [28]. FOXM1 activity is primarily regulated through post-translational phosphorylation with CDK1 being one of the kinases responsible for phosphorylating FOXM1 at specific serine and threonine residues, particularly serine 251 (S251) and threonine 611 (T611) [32, 43]. These phosphorylation events stabilize FOXM1, facilitate its nuclear localization, and enhance its transcriptional activity. While this regulatory mechanism has been well characterized in tumorigenic cell lines [32, 43], its role in NHK remains to be elucidated.

To explore the relevance of CDK1 activity in regulating FOXM1 function in NHKs, we utilized two CDK1 inhibitors: CYC202 (R-Roscovitine) and RO3306. CYC202 (hereafter referred to as CYC; Suppl. Figure 2a) is a selective cyclin-dependent kinase inhibitor, with high affinity for CDK1, while also affecting CDK2 and CDK5 (K_i = 0.65 µM, 0.7 µM, and 0.2 µM, respectively). By competitively inhibiting ATP binding, CYC blocks the kinase activity of these CDKs, leading to cell-cycle arrest and apoptosis in proliferating cancer cells [52]. It has also been employed as a CDK1 inhibitor in cancer treatments [52].

RO3306 is a potent ATP-competitive inhibitor of CDK1, showing minimal activity on CDK2/E, PKCδ, and SGK at higher concentrations (K_i = 340 nM, 318 nM, and 497 nM, respectively; Suppl. Figure 2b). In proliferating cancer cells, short-term exposure to RO3306 causes a reversible G2/M phase cell cycle arrest, while prolonged exposure (>48 h) triggers apoptosis [53].

To assess the effects of CDK1 inhibition in early passaged NHKs, we treated cells with 30 µM CYC and 30 µM RO3306 (see Methods for details). Upon CYC treatment, flow cytometry analysis revealed a slight but significant accumulation of cells in the G2/M phase, and a

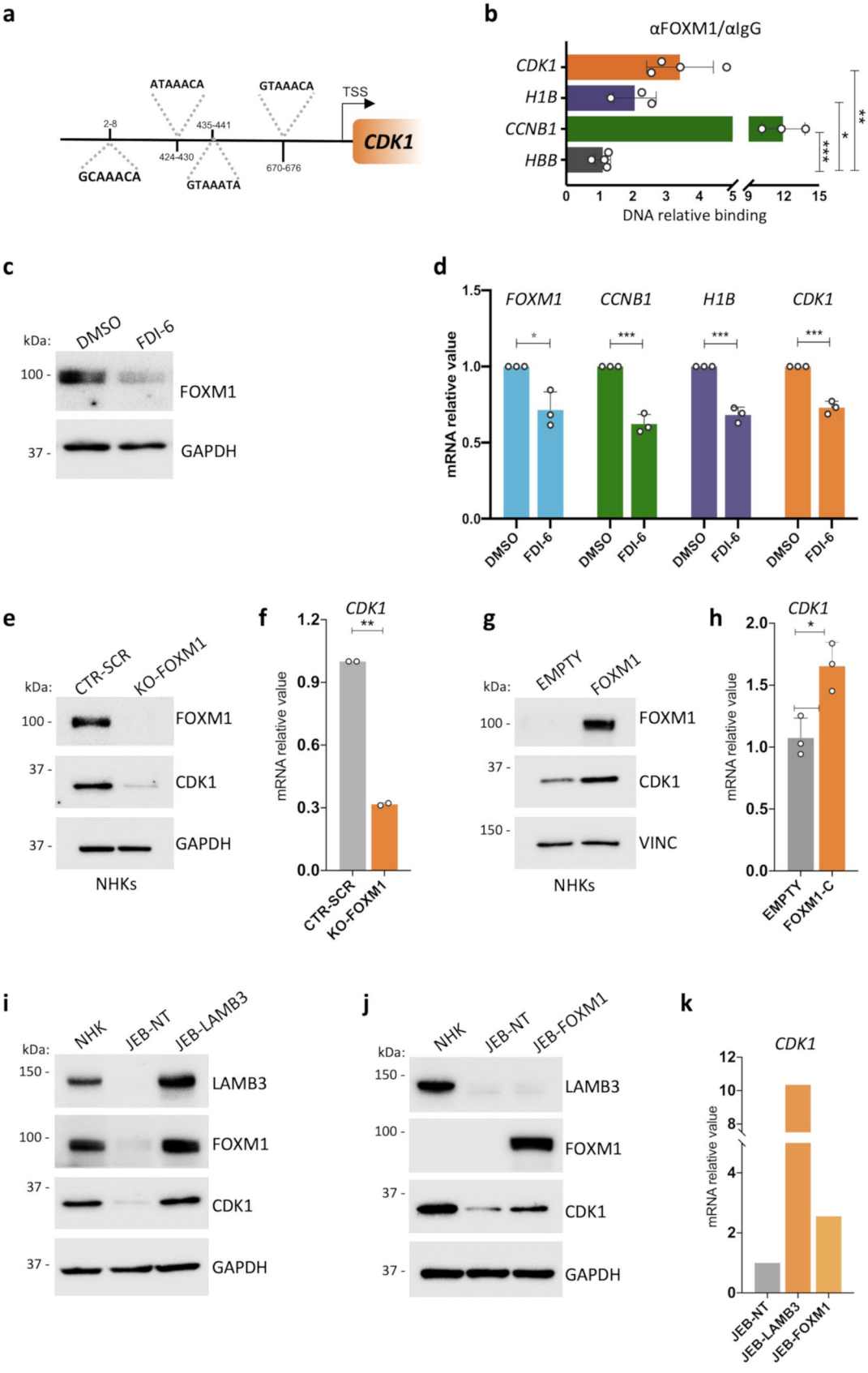

Fig. 2 (See legend on next page.)

(See figure on previous page.)

Fig. 2 A feedforward loop between FOXM1 and CDK1 in human primary epidermal cells. (**a**) Schematic representation of FOXM1 predicted binding sites on the CDK1 promoter. (**b**) ChIP-ddPCR showing FOXM1 binding to the indicated sites in NHK. Relative DNA binding was calculated as a fraction of input and normalized with the negative region (HBB, see Suppl. Table 5) arbitrarily set to 1, $N=3$ independent experiments. *$P<0.05$, **$P<0.01$ ***$P<0.001$ (Student *t*-test). (**c**) Western analysis of total cell extracts derived from NHK cultures treated with 30 μM FDI-6 or DMSO as control. Molecular weight indicators are shown. (**d**) qRT-PCR quantification of the mRNA levels of *FOXM1*, *CCNB1*, *H1B*, and *CDK1* on cells derived from DMSO- or FDI-6 -treated NHK cultures. Expression levels were normalized per *GAPDH* and given relative to the control (DMSO) arbitrarily set to 1. Data are presented as mean +/− SD of $N=3$ different independent biological replicates, *$P<0.05$, ***$P<0.001$ (Student *t*-test). (**e**) Western analysis of total cell extracts from cultures generated by primary NHKs edited with a scrambled gRNA (CTR-SCR) as control or with a gRNA specific for FOXM1 (KO-FOXM1). Molecular weight indicators are shown. (**f**) qRT-PCR quantification of the mRNA levels of *CDK1* on cells derived from gRNA scrambled- (CTR-SCR) or FOXM1-edited (KO-FOXM1) NHK. Expression levels were normalized per *GAPDH*. Data are presented as mean +/− SD of $N=2$ biological replicates, **$P<0.01$ (Student *t*-test). (**g**) Western analysis on total cell extracts derived from FOXM1- (FOXM1) or empty backbone-transduced (EMPTY) NHK cultures. FOXM1 endogenous level in NHK-empty is not detectable due to technical reasons. Molecular weight indicators are shown. (**h**) qRT-PCR quantification of the mRNA levels of *CDK1* on cells derived from FOXM1- (FOXM1) or empty backbone-transduced (EMPTY) NHK cultures. Expression levels were normalized per *GAPDH*. Data are presented as mean +/− SD of $N=3$ different independent biological replicates, *$P<0.05$ (Student *t*-test). (**i**) Western analysis on total cell extracts derived from NHK, untransduced (JEB-NT) and LAMB3-transduced (JEB-LAMB3) JEB-derived primary keratinocyte cultures. Molecular weight indicators are shown. (**j**) Western analysis on total cell extracts derived from untransduced (JEB-NT) and FOXM1-transduced (JEB-FOXM1) JEB-derived primary keratinocyte cultures. Molecular weight indicators are shown. (**k**) qRT-PCR quantification of the mRNA levels of *CDK1* on cells derived from untransduced (JEB-NT), FOXM1- (JEB-FOXM1), or LAMB3-transduced (JEB-LAMB3) JEB-derived primary keratinocyte culture. Expression levels are normalized per *GAPDH*. Data from one available patient are shown

reduction in the number of cells in G1 phase (Suppl. Figure 2c). These data suggest a partial G2/M phase arrest due to CDK1 inhibition as compared to DMSO-treated controls. In contrast, RO3306 treatment did not produce significant cell cycle alterations, suggesting that short-term inhibition of CDK1 may not be sufficient to fully disrupt cell cycle progression (Suppl. Figure 2c).

In untreated NHKs, FOXM1 protein displayed a characteristic smeared band, indicative of phosphorylation at multiple residues under physiological conditions. Upon treatment with either CYC or RO3306, a more compact FOXM1 band appeared, suggesting hypo-phosphorylation of the protein (Fig. 1f, g). This effect was not observed in cells treated with BI2536 (30 nM for 24 h), a PLK1 inhibitor that also plays a role in FOXM1 phosphorylation, though primarily in cancer cells (Suppl. Figure 2d) [54].

Interestingly, *FOXM1* mRNA levels remained unchanged following both CYC and RO3306 treatments (Fig. 1h, light blue bars). However, a decrease in FOXM1 transcriptional activity was evident, as shown by reduced mRNA levels of two FOXM1 target genes, *CCNB1* and *H1B* (Fig. 1h, green and violet bars, respectively). Additionally, *CDK1* mRNA levels decreased following CYC treatment (Fig. 1h, orange bars), although no significant reduction in its protein levels was observed (Fig. 1f).

A feedforward loop between FOXM1 and CDK1 in human primary keratinocytes

Previous studies have demonstrated that FOXM1 regulates a network of genes involved in cell-cycle progression, including *CDK1* [55, 56]. To investigate whether FOXM1 also regulates CDK1 expression in NHKs, we conducted a bioinformatic analysis identifying four predicted FOXM1 binding sites within the *CDK1* promoter region, up to 1000 bp upstream of the transcription start site (TSS) (Fig. 2a). Chromatin immunoprecipitation (ChIP) assays confirmed that FOXM1 binds to CDK1 promoter (Fig. 2b), consistently with these predictions. As internal control, we also verified that FOXM1 bound the promoter of *CCNB1* and *H1B*, FOXM1 known target genes [31].

Next, we explored the impact of modulating FOXM1 transcriptional activity on *CDK1* mRNA levels. We took advantage of the FOXM1 inhibitor FDI-6, which prevents FOXM1 from binding to its target DNA and blocks downstream gene transcription [57, 58](Suppl. Figure 3a). NHK treatment with 30 μM FDI-6 did not significantly alter cell-cycle phase distribution (Suppl. Figure 3b), but it led to a marked reduction in FOXM1 protein levels (Fig. 2c). Consistently, a reduction in FOXM1 target genes, such as *CCNB1* and *H1B*, has been observed (Fig. 2d). Notably, also *CDK1* expression was diminished, suggesting a direct transcriptional regulatory role of FOXM1 on *CDK1* (Fig. 2d, orange bars).

Interestingly, *FOXM1* mRNA levels were also reduced (Fig. 2d, light blue bars), supporting the existence of an auto-regulatory feedback loop for FOXM1. This observation is in line with previous reports showing that transcriptional inhibitors, such as Siomycin A and Thiostrepton, similarly reduce FOXM1 activity and expression [34, 59]. Furthermore, it has been shown that disruption of specific FOXM1 binding sites (−745/−738 bp) significantly diminishes FOXM1 promoter activity, emphasizing the importance of this region in FOXM1 auto-regulation [59, 60]. Further investigation is necessary to determine whether the reduction in FOXM1 protein levels following FDI-6 treatment is due to decreased transcription or alteration in protein stability.

Treatment with the CDK1 inhibitor CYC also resulted in a reduction in *CDK1* mRNA levels, although CDK1 protein levels remained unchanged (Fig. 1f, h). This observation suggests that the inhibition of FOXM1 activity caused by CYC treatment may also indirectly affect

CDK1 mRNA levels. Collectively, these findings support the notion that FOXM1 and CDK1 are engaged in a feed-forward regulatory loop. FOXM1 enhances the transcription of *CDK1*, which in turn phosphorylates and activates FOXM1, leading to increased transcriptional activity. This loop might have a crucial role in the FOXM1-dependent regulation of genes associated with EPSCs self-renewal.

CDK1 expression correlates with FOXM1 in human primary keratinocytes

To better understand the interplay between FOXM1 and CDK1, we investigated whether altering FOXM1 levels impacts *CDK1* expression. Using CRISPR-Cas9 gene-editing technology, we performed *FOXM1* genetic ablation and examined its effect on *CDK1* expression in NHKs.

A 20-nucleotide guide RNA targeting exon 2 was designed with no predicted off-target effects, as confirmed by the Cas-OFFinder tool, set to allow one mismatch and no DNA-bulge. NHKs were nucleofected with the CRISPR-Cas9 complex targeting *FOXM1*, and the genomic editing was assessed using TIDE analysis. Complete knockout of *FOXM1* was achieved with 100% editing efficiency at both alleles (Suppl. Figure 4a). Western blot analysis further confirmed the absence of FOXM1 protein (Fig. 2e). Consistent with previous findings [31], *FOXM1* knockout led to the downregulation of its well-established targets, *CCNB1* and *H1B*, and to a initial upregulation of differentiation markers (*TGM1*, *IVL*, and *SPINK5*) (Suppl. Figure 4b). Furthermore, *FOXM1* knockout resulted in a marked reduction in CDK1 expression at both the mRNA and protein levels (Fig. 2e, f).

Conversely, FOXM1 enforced expression greatly slackened physiological clonal conversion and sustained holoclone formation during serial cultivation [28]. NHKs transduced with a lentiviral vector overexpressing FOXM1 displayed a statistically significant increase in CDK1 expression at both the mRNA and protein levels (Fig. 2g, h).

To further investigate the correlation between CDK1 and FOXM1 expression in epidermal cultures, we analyzed CDK1 expression in keratinocyte cultures derived from patients with junctional epidermolysis bullosa (JEB), a severe genetic skin disorder characterized by extensive blistering due to mutations in adhesion proteins, such as Laminin-β3 and Collagen type XVII alpha 1 chain, which anchor the epidermis to the dermis [14, 61, 62]. This interaction is disrupted in JEB patients, leading to premature stem cell exhaustion during in vitro cultivation, primarily due to YAP inactivation and subsequent downregulation of downstream targets, including *FOXM1* [28, 30].

In primary keratinocytes derived from a JEB patient with two heterozygous *LAMB3* mutations (c.2242G>T and c.823-1G>T), both LAMB3 gene therapy and enforced FOXM1 expression prevented stem cell exhaustion [28, 30]. Notably, CDK1 expression was restored under both conditions (Fig. 2i-k).

CDK1 expression at single-cell level

Our data suggest a strong correlation between CDK1 expression, FOXM1 activity and percentage of stem cells in NHK. Holoclone-forming EPSCs, which are essential for long-term tissue regeneration, give rise to TACs (meroclone- and paraclone-forming cells) with progressively decreasing proliferative potential, eventually maturing into non-clonogenic, terminally differentiated cells [3, 51]. The FOXM1 pathway is upregulated in holoclones and crucial for their maintenance during in vitro cultivation [28].

To assess whether CDK1 is co-expressed with FOXM1 in the stem-cell compartment, we analyzed a published single-cell dataset from NHK. *CDK1* expression was highest in the Holoclone (H) cluster and progressively decreased across the Meroclone (M), Paraclone (P), and Terminally Differentiated (TD) clusters (Fig. 3a, b, left column, Suppl. Figure 5a). This pattern closely mirrors *FOXM1* expression (Fig. 3c, d, left column). Further analysis revealed that over 66% of cells in the H cluster contained at least one transcript of both *CDK1* and *FOXM1* (Fig. 3e, left column, Suppl. Figure 5b, c). A similar co-expression trend was observed in the transcriptome profiles from cells directly obtained from skin biopsies (Fig. 3b, d, e, right columns, Suppl. Figure 5d-f) [29, 31].

To verify whether CDK1 is predominantly expressed in the stem cell compartment, we performed clonal analysis on NHK [51]. Single-cell clones were isolated and cultured over seven days, allowing us to classify the original cell as holoclone-, meroclone-, or paraclone-forming cell. Real-time RNA analysis confirmed that *CDK1* expression was highest in holoclones (Fig. 3f, red bars), with a marked, progressive reduction in its mRNA levels as cells transitioned into mero- and paraclones (Fig. 3f, light blue bars). Western blot analysis corroborated these findings, showing highest CDK1 protein levels in holoclones, with reduced expression in mero- and paraclones (Fig. 3g).

Collectively, these results suggest that FOXM1 and CDK1 are highly expressed in EPSCs, with their expression and co-localization diminishing as the cells undergo differentiation.

Discussion

CDK1 is widely recognized for its pivotal role in cell-cycle regulation, particularly in cancer biology. Among its pleiotropic functions, our findings highlight CDK1's crucial role in regulating FOXM1 in human primary

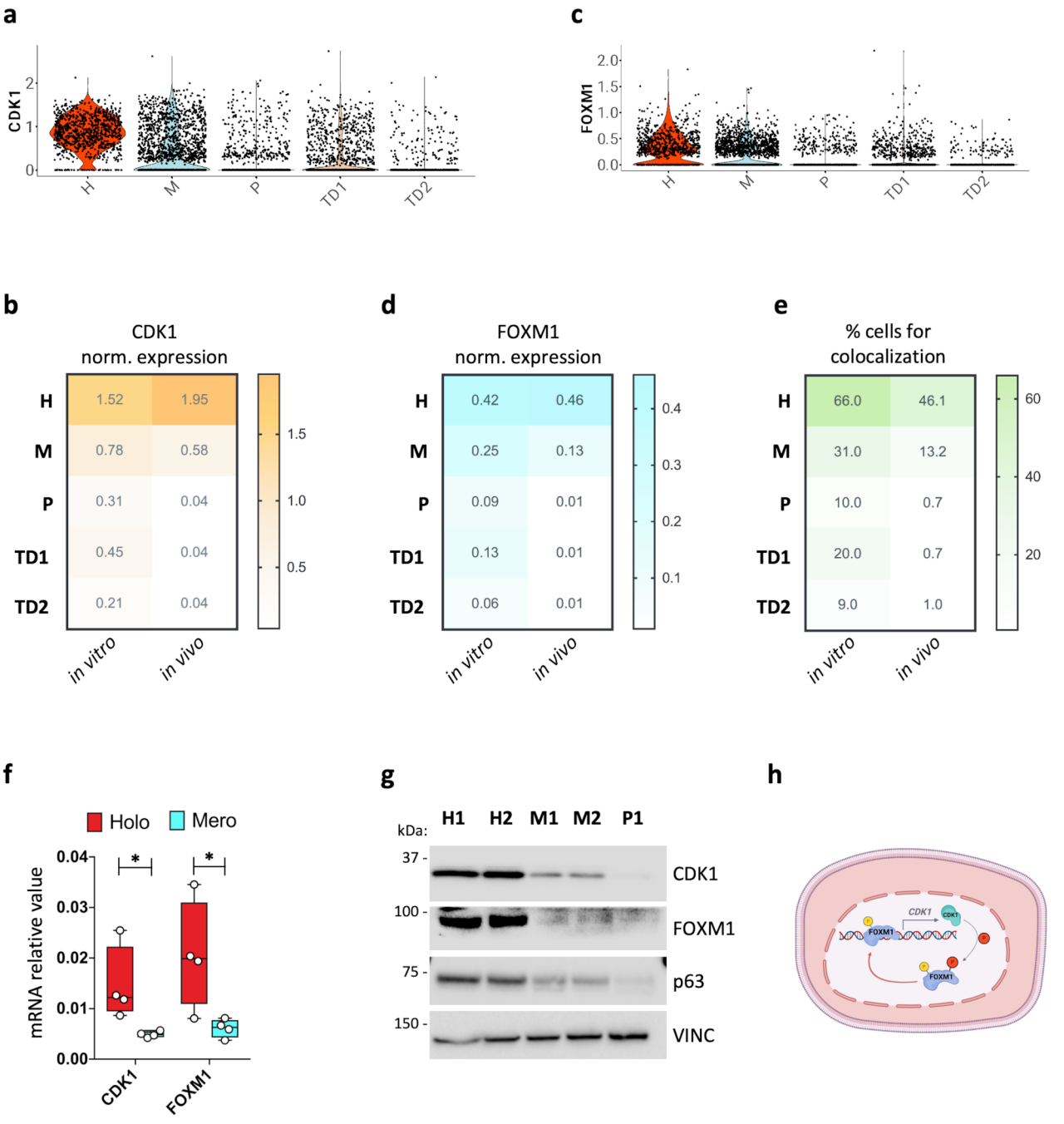

Fig. 3 CDK1 expression at single cell level. (**a**, **c**) Violin plots showing *CDK1* and *FOXM1* expression across the H, M, P, TD1 and TD2 clusters derived from scRNA-seq data from in vitro-cultured NHK. (**b**, **d**, **e**) Heatmaps showing the percentage of cells in the H, M, P, TD1, and TD2 clusters derived from scRNA-seq data from in vitro culture (left column) and from skin biopsies (right column) expressing *CDK1* (in orange), *FOXM1* (in light blue) and containing at least one transcript of both *FOXM1* and *CDK1* (in green). Expression levels are given as normalized expressions (see Methods). (**f**) qRT-PCR quantification of the mRNA levels of *CDK1* and *FOXM1* on clones generated from at least two NHK cultures. Expression levels were normalized per *GAPDH*. Holoclones and meroclones are displayed in red and light blue, respectively. Data are presented as mean +/− SD of $N = 5$ different independent biological replicates, $^*P < 0.05$ (Student *t*-test). (**g**) Western analysis of total cell extracts from cultures generated by holoclones (H1, H2), meroclones (M1, M2), and paraclone (P1) isolated by clonal analysis (see Methods) of sub-confluent NHKs. Molecular weight indicators are shown. (**h**) Schematic representation of the proposed mechanism. FOXM1 binds to *CDK1* promoter, possibly enhancing its expression. CDK1 then phosphorylates FOXM1, further promoting its activity as a transcription factor on its target genes, among which *CDK1*. Created with BioRender

keratinocytes from both healthy donors and JEB patients. We propose the existence of a feedforward loop between CDK1 and FOXM1: FOXM1 directly binds to the *CDK1* promoter inducing its expression, while CDK1, in turn, phosphorylates and activates FOXM1. This regulatory loop may function as a mechanism in sustaining FOXM1 activity, thereby supporting the self-renewal potential of EPSCs (Fig. 3h).

Our data demonstrate a strong association between CDK1 expression and the presence of stem cells within the culture. CDK1 expression is highest in holoclone-forming cells and significantly decreases as cells progress through differentiation. CDK1 and FOXM1 co-expression in EPSCs, along with their concurrent downregulation during differentiation, suggests a functional interaction between these proteins in maintaining the stem-cell state. Indeed, FOXM1 depletion results in decreased *CDK1* expression and a reduced number of holoclone-forming stem cells. Conversely, the enforced FOXM1 expression in both normal and JEB-derived keratinocytes impedes clonal conversion, preserving the stem cell compartment and high *CDK1* expression.

These findings could offer valuable insights into the biochemical mechanisms underlying the regulation of self-renewal and differentiation pathways in EPSCs. They could represent a potential therapeutic strategy, especially in those conditions where stem cell maintenance is impaired. In this context, enzyme-based therapy has recently attracted significant attention due to advancements in new encapsulation strategies [63]. By encapsulating enzymes or modifying their delivery systems, enzyme therapy could complement cell-based therapies. Indeed targeting specific biochemical pathways could enhance stem cells maintenance and function. Such strategy could be particularly beneficial in disorders characterized by impaired cellular regeneration or enzyme deficiency.

Additionally, both CDK1 and FOXM1 have been proposed as also involved in the energy metabolism, another important aspect of self-renewal maintenance [64–67]: CDK1 may directly phosphorylate metabolic enzymes or their regulators [66], whereas FOXM1 has been linked to glycolysis and to the response to reactive oxygen species (ROS) [65, 68]. Further research will focus on delineating these aspects and the specific role of CDK1 in EPSCs and TACs, eventually identifying additional components of this regulatory network.

Finally, these findings will allow a better control of the stem cell content on cultured epidermal grafts to implement the development of cell and gene therapy applications.

Supplementary Information

The online version contains supplementary material available at https://doi.org/10.1186/s13062-024-00540-8.

Supplementary Material 1

Supplementary Material 2

Supplementary Material 3

Acknowledgements

We thank all lab members for helpful feedback and comments on this manuscript. The authors acknowledge the "Fondazione Cassa di Risparmio di Modena" for funding the Exploris 480 system at the Centro Interdipartimentale Grandi Strumenti (CIGS) of the University of Modena and Reggio Emilia.

Author contributions

MPP, AR, GM, FR, GB and GAG performed experiments; MPP, AR analyzed data, assembled all input data and edited the manuscript; GM conducted bioinformatics analyses; LZ, MPC performed mass spectrometry experiments and analyzed data. EE coordinated the study, defined strategic procedures, administered the experiments, and wrote the manuscript.

Funding

This research was funded by the Project PRIN 2022 2022KRTKXS CUP E53D23007430006 "High-resolution study of translational dynamics in human epithelial stem cells" within the National Recovery and Resilience Plan (NRRP), Mission 4, Component 2 Investment 1.1. for the National Research Program (PNR) and Research Projects of Significant National Interest (PRIN)", funded by the European Union – NextGenerationEU - ref. D.D. No.104 of 02/02/2022 to EE.

Data availability

scRNA-seq data have been deposited in the Gene Expression Omnibus database under accession code GSE155817, referring to article [9]. scRNA-seq data of in vivo biopsies are published in [11]. Raw data (normalized protein intensity values) of the Label Free MS Proteomics experiment and the differentially expressed proteins (DEPs) is available in Open Access on the FairDom repository at https://fairdomhub.org/data_files/7500. We declare that the data supporting the findings of this study are available within the paper and from the authors upon request.

Declarations

Competing interests

The authors declare no competing interests.

Received: 23 September 2024 / Accepted: 7 October 2024
Published online: 13 October 2024

References

1. Watt FM. Stem cell fate and patterning in mammalian epidermis. Curr Opin Genet Dev. 2001;11(4):410–7.
2. Watt FM. The stem cell compartment in human interfollicular epidermis. J Dermatol Sci. 2002;28(3):173–80.
3. Hirsch T, Rothoeft T, Teig N, Bauer JW, Pellegrini G, De Rosa L, et al. Regeneration of the entire human epidermis using transgenic stem cells. Nature. 2017;551(7680):327–32.
4. Pellegrini G, Golisano O, Paterna P, Lambiase A, Bonini S, Rama P, et al. Location and clonal analysis of stem cells and their differentiated progeny in the human ocular surface. J Cell Biol. 1999;145(4):769–82.
5. Rochat A, Kobayashi K, Barrandon Y. Location of stem cells of human hair follicles by clonal analysis. Cell. 1994;76(6):1063–73.
6. Blanpain C, Fuchs E. Epidermal stem cells of the skin. Annu Rev Cell Dev Biol. 2006;22:339–73.
7. Blanpain C, Fuchs E. Plasticity of epithelial stem cells in tissue regeneration. Science. 2014;344(6189):1242281.

8. Gallico GG, O'Connor NE, Compton CC, Kehinde O, Green H. Permanent coverage of large burn wounds with autologous cultured human epithelium. N Engl J Med. 1984;311(7):448–51.
9. Rama P, Matuska S, Paganoni G, Spinelli A, De Luca M, Pellegrini G. Limbal stem-cell therapy and long-term corneal regeneration. N Engl J Med. 2010;363(2):147–55.
10. Pellegrini G, Traverso CE, Franzi AT, Zingirian M, Cancedda R, De Luca M. Long-term restoration of damaged corneal surfaces with autologous cultivated corneal epithelium. Lancet. 1997;349(9057):990–3.
11. Mavilio F, Pellegrini G, Ferrari S, Di Nunzio F, Di Iorio E, Recchia A, et al. Correction of junctional epidermolysis bullosa by transplantation of genetically modified epidermal stem cells. Nat Med. 2006;12(12):1397–402.
12. Sercia L, Romano O, Marini G, Enzo E, Forcato M, De Rosa L, et al. A cellular disease model towards gene therapy of TGM1-dependent Lamellar Ichthyosis. Volume 101311. Molecular Therapy - Methods & Clinical Development; 2024.
13. Cattaneo C, Enzo E, De Rosa L, Sercia L, Consiglio F, Forcato M, et al. Allele-specific CRISPR-Cas9 editing of dominant epidermolysis bullosa simplex in human epidermal stem cells. Mol Ther. 2024;32(2):372–83.
14. De Rosa L, Enzo E, Zardi G, Bodemer C, Magnoni C, Schneider H, et al. Hologene 5: a phase II/III clinical trial of combined cell and gene therapy of junctional epidermolysis bullosa. Front Genet. 2021;12:705019.
15. Zhang L, Piipponen M, Liu Z, Li D, Bian X, Niu G, et al. Human skin specific long noncoding RNA HOXC13-AS regulates epidermal differentiation by interfering with Golgi-ER retrograde transport. Cell Death Differ. 2023;30(5):1334–48.
16. Hu Ydou, Wu K, Liu Y, jie, Zhang Q, Shen H, Ji J, et al. LY6/PLAUR domain containing 3 (LYPD3) maintains melanoma cell stemness and mediates an immunosuppressive microenvironment. Biol Direct. 2023;18(1):72.
17. Pinto NA, Abba MC, Laporte L, Pérez Sáez JM, Blidner AG, Torres NI, et al. Galectin-7 reprograms skin carcinogenesis by fostering innate immune evasive programs. Cell Death Differ. 2023;30(4):906–21.
18. Cappello A, Mancini M, Madonna S, Rinaldo S, Paone A, Scarponi C, et al. Extracellular serine empowers epidermal proliferation and psoriasis-like symptoms. Sci Adv. 2022;8(50):eabm7902.
19. Pecorari R, Bernassola F, Melino G, Candi E. Distinct interactors define the p63 transcriptional signature in epithelial development or cancer. Biochem J. 2022;479(12):1375–92.
20. Barrandon Y, Green H. Three clonal types of keratinocyte with different capacities for multiplication. Proc Natl Acad Sci U S A. 1987;84(8):2302–6.
21. Mills AA, Zheng B, Wang XJ, Vogel H, Roop DR, Bradley A. p63 is a p53 homologue required for limb and epidermal morphogenesis. Nature. 1999;398(6729):708–13.
22. Yang A, Schweitzer R, Sun D, Kaghad M, Walker N, Bronson RT, et al. p63 is essential for regenerative proliferation in limb, craniofacial and epithelial development. Nature. 1999;398(6729):714–8.
23. Viticchiè G, Agostini M, Lena AM, Mancini M, Zhou H, Zolla L, et al. p63 supports aerobic respiration through hexokinase II. Proc Natl Acad Sci USA. 2015;112(37):11577–82.
24. Li Y, Giovannini S, Wang T, Fang J, Li P, Shao C, et al. p63: a crucial player in epithelial stemness regulation. Oncogene. 2023;42(46):3371–84.
25. Mancini M, Sergio S, Cappello A, Farkas T, Bernassola F, Scarponi C, et al. Involvement of transcribed lncRNA uc.291 in hyperproliferative skin disorders. Biol Direct. 2023;18:82.
26. Pellegrini G, Dellambra E, Golisano O, Martinelli E, Fantozzi I, Bondanza S, et al. p63 identifies keratinocyte stem cells. Proc Natl Acad Sci. 2001;98(6):3156–61.
27. Smirnov A, Lena AM, Tosetti G, Yang X, Cappello A, Citterich MH, et al. Epigenetic priming of an epithelial enhancer by p63 and CTCF controls expression of a skin-restricted gene XP33. Cell Death Discov. 2023;9(1):1–9.
28. Enzo E, Secone Seconetti A, Forcato M, Tenedini E, Polito MP, Sala I, et al. Single-keratinocyte transcriptomic analyses identify different clonal types and proliferative potential mediated by FOXM1 in human epidermal stem cells. Nat Commun. 2021;12(1):2505.
29. Polito MP, Marini G, Palamenghi M, Enzo E. Decoding the human epidermal complexity at single-cell resolution. Int J Mol Sci. 2023;24(10):8544.
30. De Rosa L, Secone Seconetti A, De Santis G, Pellacani G, Hirsch T, Rothoeft T, et al. Laminin 332-dependent YAP dysregulation depletes epidermal stem cells in junctional Epidermolysis bullosa. Cell Rep. 2019;27(7):2036–e20496.
31. Polito MP, Marini G, Fabrizi A, Sercia L, Enzo E, De Luca M. Biochemical role of FOXM1-dependent histone linker H1B in human epidermal stem cells. Cell Death Dis. 2024;15(7):508.
32. Wierstra I, Alves J. FOXM1c is activated by cyclin E/Cdk2, cyclin A/Cdk2, and cyclin A/Cdk1, but repressed by GSK-3α. Biochem Biophys Res Commun. 2006;348(1):99–108.
33. Major ML, Lepe R, Costa RH. Forkhead box M1B transcriptional activity requires binding of cdk-cyclin complexes for phosphorylation-dependent recruitment of p300/CBP coactivators. Mol Cell Biol. 2004;24(7):2649–61.
34. Liao GB, Li XZ, Zeng S, Liu C, Yang SM, Yang L, et al. Regulation of the master regulator FOXM1 in cancer. Cell Commun Signal. 2018;16(1):57.
35. Lim S, Kaldis P. Cdks, cyclins and CKIs: roles beyond cell cycle regulation. Development. 2013;140(15):3079–93.
36. Malumbres M. Cyclin-dependent kinases. 2014.
37. Santamaría D, Barrière C, Cerqueira A, Hunt S, Tardy C, Newton K, et al. Cdk1 is sufficient to drive the mammalian cell cycle. Nature. 2007;448(7155):811–5.
38. Massacci G, Perfetto L, Sacco F. The cyclin-dependent kinase 1: more than a cell cycle regulator. Br J Cancer. 2023;129(11):1707–16.
39. Cdk1 interplays with Oct4. to repress differentiation of embryonic stem cells into trophectoderm - Li – 2012 - FEBS Letters - Wiley Online Library. [cited 2024 Sep 19]. https://febs.onlinelibrary.wiley.com/doi/full/https://doi.org/10.1016/j.febslet.2012.10.030
40. Ali F, Hindley C, McDowell G, Deibler R, Jones A, Kirschner M, et al. Cell cycle-regulated multi-site phosphorylation of neurogenin 2 coordinates cell cycling with differentiation during neurogenesis. Development. 2011;138(19):4267–77.
41. Kitzmann M, Vandromme M, Schaeffer V, Carnac G, Labbé JC, Lamb N, et al. cdk1- and cdk2-Mediated phosphorylation of MyoD Ser200 in growing C2 myoblasts: role in modulating MyoD half-life and myogenic activity. Mol Cell Biol. 1999;19(4):3167–76.
42. Neganova I, Tilgner K, Buskin A, Paraskevopoulou I, Atkinson SP, Peberdy D, et al. CDK1 plays an important role in the maintenance of pluripotency and genomic stability in human pluripotent stem cells. Cell Death Dis. 2014;5(11):e1508–1508.
43. Chen YJ, Dominguez-Brauer C, Wang Z, Asara JM, Costa RH, Tyner AL, et al. A conserved phosphorylation site within the Forkhead domain of FoxM1B is required for its activation by cyclin-CDK1. J Biol Chem. 2009;284(44):30695–707.
44. Branigan TB, Kozono D, Schade AE, Deraska P, Rivas HG, Sambel L, et al. MMB-FOXM1-driven premature mitosis is required for CHK1 inhibitor sensitivity. Cell Rep. 2021;34(9):108808.
45. Todaro GJ, Green H. Quantitative studies of the growth of mouse embryo cells in culture and their development into established lines. J Cell Biol. 1963;17(2):299–313.
46. D'Arca D, Severi L, Ferrari S, Dozza L, Marverti G, Magni F, et al. Serum mass spectrometry proteomics and protein set identification in response to FOLFOX-4 in drug-resistant ovarian carcinoma. Cancers (Basel). 2023;15(2):412.
47. Orsburn BC. Proteome discoverer—a community enhanced data processing suite for protein informatics. Proteomes. 2021;9(1):15.
48. UniProt Consortium. The universal protein resource (UniProt). Nucleic Acids Res. 2008;36(Database issue):D190–195.
49. Mellacheruvu D, Wright Z, Couzens AL, Lambert JP, St-Denis NA, Li T, et al. The CRAPome: a contaminant repository for affinity purification-mass spectrometry data. Nat Methods. 2013;10(8):730–6.
50. Sadygov RG. Using SEQUEST with theoretically complete sequence databases. J Am Soc Mass Spectrom. 2015;26(11):1858–64.
51. Enzo E, Cattaneo C, Consiglio F, Polito MP, Bondanza S, De Luca M. Clonal analysis of human clonogenic keratinocytes. In: Methods in Cell Biology. Elsevier; 2022 [cited 2022 Aug 26]. pp. 101–16. https://linkinghub.elsevier.com/retrieve/pii/S0091679X22000267
52. Wang Q, Bode AM, Zhang T. Targeting CDK1 in cancer: mechanisms and implications. npj Precis Onc. 2023;7(1):58.
53. Vassilev LT, Tovar C, Chen S, Knezevic D, Zhao X, Sun H, et al. Selective small-molecule inhibitor reveals critical mitotic functions of human CDK1. Proc Natl Acad Sci USA. 2006;103(28):10660–5.
54. Fu Z, Malureanu L, Huang J, Wang W, Li H, Van Deursen JM, et al. Plk1-dependent phosphorylation of FoxM1 regulates a transcriptional programme required for mitotic progression. Nat Cell Biol. 2008;10(9):1076–82.
55. Laoukili J, Kooistra MRH, Brás A, Kauw J, Kerkhoven RM, Morrison A, et al. FoxM1 is required for execution of the mitotic programme and chromosome stability. Nat Cell Biol. 2005;7(2):126–36.
56. Kang K, Choi Y, Kim HH, Yoo KH, Yu S. Predicting FOXM1-mediated gene regulation through the analysis of genome-wide FOXM1 binding sites in MCF-7,

K562, SK-N-SH, GM12878 and ECC-1 cell lines. Int J Mol Sci. 2020 [cited 2021 May 6];21(17). https://www.ncbi.nlm.nih.gov/pmc/articles/PMC7503762/
57. Gormally MV, Dexheimer TS, Marsico G, Sanders DA, Lowe C, Matak-Vinković D, et al. Suppression of the FOXM1 transcriptional programme via novel small molecule inhibition. Nat Commun. 2014;5(1):5165.
58. Wang SP, Wu SQ, Huang SH, Tang YX, Meng LQ, Liu F, et al. FDI-6 inhibits the expression and function of FOXM1 to sensitize BRCA-proficient triple-negative breast cancer cells to olaparib by regulating cell cycle progression and DNA damage repair. Cell Death Dis. 2021;12(12):1138.
59. Halasi M, Gartel AL. A novel mode of FoxM1 regulation: positive auto-regulatory loop. Cell Cycle. 2009;8(12):1966–7.
60. Chen X, Müller GA, Quaas M, Fischer M, Han N, Stutchbury B, et al. The forkhead transcription factor FOXM1 controls cell cycle-dependent gene expression through an atypical chromatin binding mechanism. Mol Cell Biol. 2013;33(2):227–36.
61. De Rosa L, Enzo E, Palamenghi M, Sercia L, De Luca M. Stairways to advanced therapies for epidermolysis bullosa. Cold Spring Harb Perspect Biol. 2022;15(4):a041229.
62. Chakravarti S, Enzo E, de Barros M, Rizzarda Mafezzoni B, Pellegrini G. Genetic disorders of the extracellular matrix: from cell and gene therapy to future applications in regenerative medicine. 2022; Annual Review of Genomics and Human Genetic, review.
63. Cuoghi S, Caraffi R, Anderlini A, Baraldi C, Enzo E, Vandelli MA, et al. Challenges of enzyme therapy: why two players are better than one. Wiley Interdiscip Rev Nanomed Nanobiotechnol. 2024;16(4):e1979.
64. Polito MP, Romaldini A, Rinaldo S, Enzo E. Coordinating energy metabolism and signaling pathways in epithelial self-renewal and differentiation. Biol Direct. 2024;19(1):63.
65. Cheng Y, Sun F, Thornton K, Jing X, Dong J, Yun G, et al. FOXM1 regulates glycolysis and energy production in multiple myeloma. Oncogene. 2022;41(32):3899–911.
66. Solaki M, Ewald JC. Fueling the cycle: CDKs in carbon and energy metabolism. Front Cell Dev Biol. 2018;6:93.
67. Santinon G, Enzo E, Dupont S. The sweet side of YAP/TAZ. Cell Cycle. 2015;14(16):2543–4.
68. Smirnov A, Panatta E, Lena A, Castiglia D, Di Daniele N, Melino G, et al. FOXM1 regulates proliferation, senescence and oxidative stress in keratinocytes and cancer cells. Aging. 2016;8(7):1384–97.

Publisher's note